RSC Advances

PAPER

View Article Online
View Journal | View Issue



Cite this: *RSC Adv.*, 2019, **9**, 29967

# Barrier thickness dependence of $Mg_xZn_{1-x}O$/ZnO quantum well (QW) on the performance of a p-NiO/QW/n-ZnO photodiode

Jun Dar Hwang * and Jhong Yung Jiang

An $Mg_xZn_{1-x}O$/ZnO quantum well (QW) structure, with various barrier ($Mg_xZn_{1-x}O$ layer) thicknesses, was inserted into p-NiO/n-ZnO heterojunction photodiodes (HPDs) by using a radio-frequency magnetron sputtering system. The effect of various barrier thicknesses on the performance of QW-PDs was investigated. A band diagram shows that the QW-PD with 10 nm barrier layer presents a tunneling carrier transport mechanism, the UV- and visible-generated carriers tunnel through the thin barrier layer. Whereas the QW-PDs with thicker (≧25 nm) barrier layers show recombination-tunneling carrier transport. The visible-generated carriers are effectively confined within the well layer in the QW structure, causing the visible-response to be greatly reduced by more than 3 orders compared to that in the QW-PD with a 10 nm barrier layer. However, on further increasing the barrier thickness beyond 25 nm, the visible-response will no longer be reduced. In contrast, with decreasing the barrier thickness from 60 to 25 nm, the UV-response increases due to the overlap increase of the fundamental electron and hole wave function in the quantum well. Such a result drastically enhances the rejection ratio (320 nm/500 nm) from 264 for QW-PDs with a 10 nm barrier to 2986 for QW-PDs with a 25 nm barrier layer by a 11.3 ratio.

Received 7th August 2019
Accepted 11th September 2019

DOI: 10.1039/c9ra06131b

rsc.li/rsc-advances



## Introduction

ZnO-based materials are attractive semiconductors for fabricating ultraviolet (UV) photodetectors, such as p–n, Schottky-barrier, and metal–semiconductor–metal structures,[1–12] due to the advantages of wide band gap (3.2 eV), high transparency (>80%) in the visible wavelength region, high exciton binding energy (60 meV), and non-toxicity.[13,14] The addition of a Mg atom in ZnO leads to the formation of $Mg_xZn_{1-x}O$ with a band gap tuneable from 3.2 to 7.8 eV.[1,15] However, the deep acceptor levels, low dopant solubility, and self-compensation in ZnO result in a reproducible and reliable p-type ZnO being not available.[16] As a replacement for p-ZnO, p-NiO has been employed to fabricate p-NiO/n-ZnO heterojunction optoelectronics devices.[17–25] NiO is an important p-type material with a direct wide band-gap of 3.0–4.0 eV and has merits of low-cost, earth advanced, and environmental friendliness for advanced photoelectric device applications.[26–28] In spite of the developments in p-NiO/n-ZnO optoelectronic devices, many imperfections, such as oxygen vacancies in ZnO[29,30] and nickel interstitials in NiO,[22–31] are present at the NiO/ZnO heterojunction interface. These imperfections introduce large leakage current and visible response,[32] which lower rectification[29] and UV/visible rejection ratio in the p-NiO/n-ZnO heterojunction photodiodes (HPDs).[32,33]

Quantum well (QW) structures have been applied in $In_xGa_{1-x}N$/GaN and $Al_xGa_{1-x}N$/GaN photodetectors to lower leakage current and enhance UV/visible rejection ratio, because the carriers generated by low-energy photons are confined in the QW.[34,35] The barrier layer thickness in QW affect the exciton localization and piezoelectric field in the well, as well as the carrier transport and distribution in active layer.[36] Such issues play a crucial role in determining the structure and optical qualities of QW. Effect of different barrier layer thickness on the $In_xGa_{1-x}N$/GaN QW opto-electronic devices were studied, including light-emitting diodes, solar cells and photodetectors.[37–41] Previously, most $Mg_xZn_{1-x}O$/ZnO QW were studied in optical and structural properties.[42–52] $Mg_xZn_{1-x}O$/ZnO QW was employed to investigate light-polarization[53] and light-emitting diodes.[54,55] The application of $Mg_xZn_{1-x}O$/ZnO QW in photodetector is less to our knowledge. For a QW design, it is desirable to have a thinner barrier thickness. Because for a given total QW thickness, a thinner barrier leads to higher absorption due to more wells. However a thinner barrier cannot effectively confine the generated electrons and holes in the well layer, which causes a large leakage current and visible response in UV photodetectors. It is therefore useful to seek a critical barrier thickness, while maintaining a low leakage current and achieving high performance in photodetectors.

*Department of Electrophysics, National Chiayi University, No. 300 Syuefu Rd., Chiayi City 60004, Taiwan. E-mail: jundar@mail.ncyu.edu.tw*

In this work, an $Mg_xZn_{1-x}O$/ZnO QW structure with various barrier thickness was inserted into p-NiO/n-ZnO HPDs using a low-cost radio-frequency (RF) magnetron sputtering system. The effect of various barrier layer ($Mg_xZn_{1-x}O$) thickness on the performance of p-NiO/QW/n-ZnO QW-PDs was studied in detail.

## Experimental

After cleaning, the ITO/glass substrates were loaded into RF-magnetron sputtering system to deposit a 300 nm-thick ZnO layer. Next, $Mg_xZn_{1-x}O$/ZnO/$Mg_xZn_{1-x}O$ QW structured layers were consecutively deposited onto the ZnO layer using the same system.[56] The barrier layer thickness of $Mg_xZn_{1-x}O$ varies from 10, 25, 40, to 60 nm, while the well layer thickness of ZnO keeps at 4 nm. Finally, the p-NiO with a thickness of 80 nm was deposited using the same RF sputtering system as a hole transport layer.[25] The p-NiO/QW/n-ZnO QW-PDs were fabricated by evaporating Ni electrode with a interdigitated pattern onto the NiO surface. A schematic diagram of the prepared QW-PDs is shown in Fig. 1. The QW-PDs with barrier thickness of 10, 25, 40, and 60 nm are denoted as PD_A, PD_B, PD_C, and PD_D, respectively. The current–voltage (*I–V*) characteristic and photoresponse were measured using a Keithley 2400 source meter and a 300 W Xe arc lamp with monochromator.

## Results and discussion

The Mg content of the $Mg_xZn_{1-x}O$ film was measured by X-ray photoelectron spectroscopy and the film composition was determined to be $Mg_{0.3}Zn_{0.7}O$.[11] The absorption measurement showed the bandgap of $Mg_{0.3}Zn_{0.7}O$, ZnO and NiO films to be 3.7, 3.25, and 3.15 eV, respectively.[11,57] Fig. 2 shows the spectral responsivity as a function of the illumination wavelengths for the fabricated QW-PDs at a 2 V reverse-bias voltage. From the figure, a significant difference occurs between PD_A and the other QW-PDs; that is, the PD_A (with 10 nm-thick barrier layer) exhibits a higher responsivity than the other QW-PDs (PD_B ~ PD_D). The PD_B, PD_C, and PD_D have similar responsivity for various wavelengths. This suggests that the PD_B, PD_C, and PD_D are subject to the same carrier transport mechanism, and differ from that of PD_A. The photogenerated carriers are

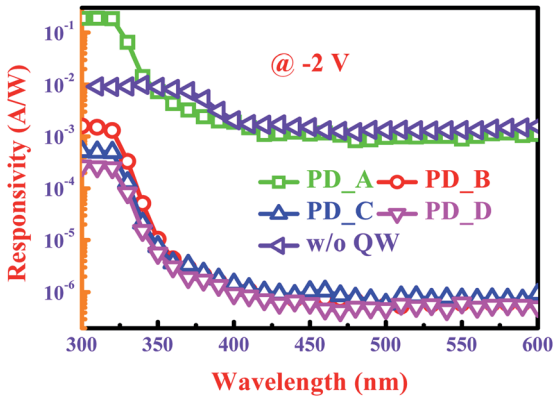


Fig. 2 Spectral responsivity as a function of illumination wavelengths for the fabricated QW-PDs biased at 2 V reverse-bias voltage.

easy to tunnel the thin (10 nm) barrier layer in PD_A and hence a higher responsivities. The PDs without a QW (w/o QW) structure is also illustrated in Fig. 2 for comparison. The PDs without a QW demonstrates a similar responsivity to PD_A for the wavelengths longer than 400 nm due to the thin barrier layer in PD_A. The PDs without a QW reveals only an absorption band for the wavelengths less than 400 nm, attributing to the absorption of ZnO. However the PDs with QW exhibits another sharply rising responsivity for the wavelengths smaller than 350 nm because the absorption of MgZnO layer. The blue shift of absorption wavelength in MgZnO, compared to that of ZnO, is a result of the introduction of Mg atom.[11]

Fig. 3 shows the responsivity *versus* various reverse-bias voltages responding to the incident wavelengths of 320 and 500 nm. With increasing reverse-bias voltage, the responsivities of all QW-PDs increase. Both the responsivities (320 and 500 nm) of PD_A demonstrate a high dependence on the bias-voltages; however a less dependence is observed in the PD_B ~ PD_D. The result reveals that the photogenerated carriers tunnel through the thin barrier layer in PD_A; in contrast, the photogenerated carriers are confined within the well layer in PD_B ~ PD_D. Compared to the visible response of the PD_A ($5.5 \times 10^{-3}$ A $W^{-1}$), the visible response of PD_B is drastically

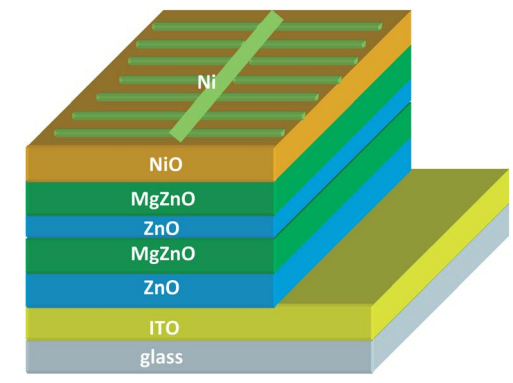


Fig. 1 Schematic diagram of the prepared QW-PD.

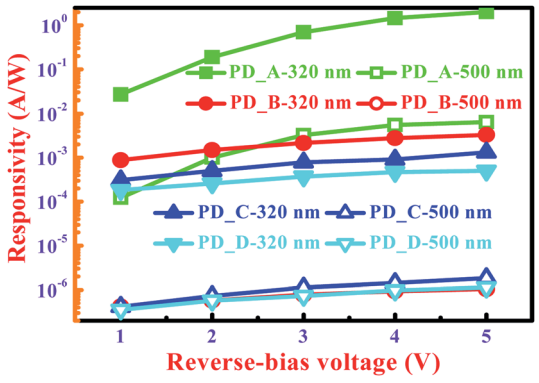


Fig. 3 Responsivity *versus* various reverse-bias voltages responding to incident wavelength of 320 and 500 nm.

reduced to 9.3 × $10^{-7}$ A $W^{-1}$ by about 4 orders at 4 V reverse-bias voltage. This is consistent with previous experiments in which the current is carried by inter-well tunnelling in a QW-PD with 10 nm barrier layer, while the inter-well tunnelling is nearly negligible for the barrier layer larger than 20 nm.[37] It was reported that the thicker barrier layer can suppress leakage current; however further increasing the barrier thickness beyond a certain value, the leakage current and visible-response will no longer be reduced.[58] This leads to the PD_B, PD_C, and PD_D exhibit almost the same visible response, shown in Fig. 3. In contrast, the UV (320 nm) response is separated in the PD_B, PD_C, and PD_D. With decreasing the barrier thickness of QW-PDs from 60 nm to 25 nm, the UV response increases. For a thick barrier layer (60 nm), the UV response of PD_D is 4.7 × $10^{-4}$ A $W^{-1}$ and it is raised to 2.8 × $10^{-3}$ A $W^{-1}$ for the 25 nm barrier layer (PD_B) at 4 V reverse-bias voltage. Also from the figure, the PD_B, PD_C, and PD_D appear the same slopes in responsivity *versus* bias-voltage, and the slope is sharply different from that of the PD_A. Such a result again evidences the PD_B, PD_C, and PD_D exhibit the same carrier transport mechanism, and differ from that of PD_A.

The rejection ratio is defined as the responsivity at 320 nm divided by that at 500 nm. Fig. 4 shows the rejection ratio for the QW-PDs at a 4 V reverse-bias voltage. Clearly, the PD_B, PD_C, and PD_D presents a larger rejection ratio than the PD_A. The PD_B (25 nm barrier layer) exhibits the largest rejection ratio. The rejection ratio is largely enhanced from 264 to 3070 for the PD_A and PD_B, respectively, by a 11.6 times higher. This means that a suitable thickness barrier layer can greatly reduce the visible response and increase the rejection ratio. From Fig. 4, the PDs without a QW presents the lowest rejection ratio than those with QW. It means the insertion of QW strongly reduces the visible response and hence the QW-PDs exhibits a higher noise rejection ability than the PDs without QW. In order to study the different carrier transport mechanism between the QW-PDs with thin (10 nm) and thick (≧25 nm) barrier layers. The dark *I*–*V* characteristics for the PD_A (with 10 nm barrier layer) and PD_B (with 25 nm barrier layer) are shown in Fig. 5. A rather leaky *I*–*V* behaviour is observed in the PD_A, while the PD_B exhibits a good rectifying characteristic.

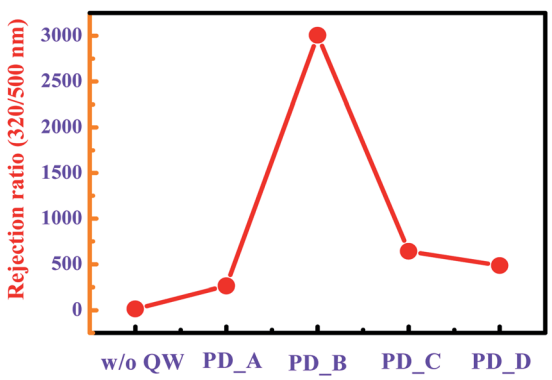


Fig. 4 Rejection ratio for the all QW-PDs biased at 4 V reverse-bias voltage.

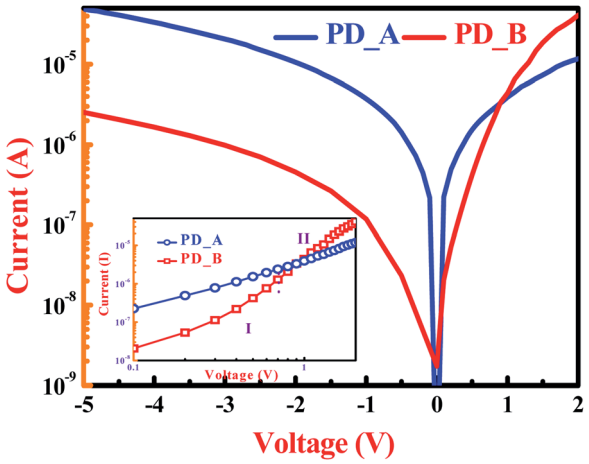


Fig. 5 Dark *I*–*V* characteristics for the PD_A and PD_B. The inset is ln(*I*) *versus* ln(*V*) for PD_A and PD_B, biased at forward-voltage.

It is well known that the leakage current (reverse-bias) is originated form thermally generated carriers. The thermally generated carriers can tunnel through the thin (10 nm) barrier layer, but are effectively confined within the well layer by the thick (≧25 nm) barrier in the $Mg_xZn_{1-x}O$/ZnO QW structure.[59] The inset of Fig. 5 shows the ln(*I*) *versus* ln(*V*) plot for the PD_A and PD_B, biased at forward voltage. For the entire voltage range, the current of the PD_A exhibits a linear dependence on bias-voltage, indicating that the carrier transport is dominated by tunnelling.[60–62] However, there are two distinct regimes in the PD_B. At low forward voltages ($V \leqq 0.7$ V), referred to as regime I, the current increases exponentially, according to the relation $I \sim \exp(\alpha V)$, where $\alpha$ is a constant. The current transport shows a recombination-tunnelling mechanism, which is usually observed in wide band gap p–n diodes.[63,64] At higher forward voltages ($V \geqq 0.7$ V), referred to as regime II, the *I*–*V* characteristic follows a power law ($I \sim V^m$), which is generally attributed to a space-charge-limited current (SCLC) conduction. The $m$ value is estimated to be 2.6. The high value of $m$ (≧2), indicates SCLC conduction with exponential trap distribution.[62]

We also investigated the reverse-bias voltage regime, at which QW-PDs are normally operated. In this regime, the ln(*I*) is plotted as a function of the reciprocal of the electrical field *E*, as shown in Fig. 6. Both PD_A and PD_B present a good linear dependence of ln(*I*) on 1/*E*, which is described well by a trap-assisted tunnelling (TAT) mechanism.[39,65] The trap-assisted tunnelling current $J_{TAT}$ is expressed as:

$$J_{TAT} = A \exp\left(\frac{-8\pi\sqrt{2qm^*}}{3hE}\varphi_r^{3/2}\right)$$

where $A$ is a constant, $m^*$ is the electron effective mass, $q$ is the elementary charge, $h$ is the Plank's constant, and $\varphi_r$ is the trap energy of the conduction band edge. Assuming that the electron effective mass in the QW is the same as in the ZnO ($0.3m_0$),[66] the trap energies are estimated to be 0.196 and 0.21 eV for the PD_A and PD_B, respectively. These trap energies are approximately equal to each other and to the 0.206 eV reported for the

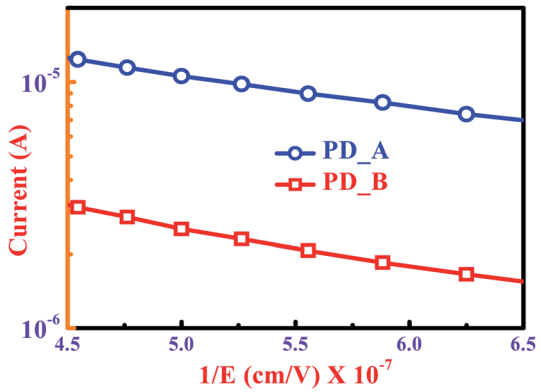


Fig. 6 ln(*I*) as a function of the reciprocal of the electrical field *E* for PD_A and PD_B, biased at reverse-voltage.

$Mg_xZn_{1-x}O$/ZnO deposited by plasma-assisted molecular-beam epitaxy.[67] This indicates that the $Mg_xZn_{1-x}O$/ZnO QW have the same quality regardless of the different $Mg_xZn_{1-x}O$ barrier layer thickness.

Therefore, the tunnelling mechanism in the PD_A is attributed to the thinness of the barrier layer (10 nm) rather than the quality of the QW.

Based on above investigations, the band diagrams of the QW-PDs with thin (10 nm) and thick (≧25 nm) barrier layers, biased at reverse-voltage, are shown in Fig. 7(a) and (b), respectively, to elucidate the different carrier transport mechanisms. In Fig. 7(a), the visible light incident on the QW-PDs with 10 nm barrier layer is absorbed by the band-gap defects of MgZnO (denoted as process 1) and ZnO (denoted as process 2), however the UV light is absorbed by a band-to-band mechanism (denoted as process 3). Both photo-generated carriers tunnel through the thin barrier layer (10 nm), leading to higher visible and UV responses compared to the QW-PDs with thicker (≧25 nm) barrier layer. The band diagram (Fig. 7(b)) illustrates that, as the barrier thickness increases to 25 nm or more, the carriers generated from the visible light from MgZnO (denoted as process 4) and ZnO (denoted as process 5) are effectively confined within the well layer in the $Mg_xZn_{1-x}O$/ZnO QW structure, which reduces the visible response by more than 3 orders compared to the QW-PD with the 10 nm barrier layer. Increasing the barrier thickness beyond a certain value (25 nm) will no longer reduce the visible response, causing the QW-PDs with thicker (≧25 nm) barrier layer to have similar visible responses, as shown in Fig. 3. In contrast, some of the carriers generated from UV light tunnel through the barrier by trap assistance (denoted as process 6) due to the carriers having higher energy than those generated by visible light. When decreasing the barrier thickness of the QW-PDs from 60 to 25 nm, the overlap of the fundamental electron and hole wave function in the quantum well increase and the carriers extraction by the trap-assisted tunnelling is enhanced.[40,41,68] The issue leads to the enhancement of UV response with decreasing barrier thickness from 60 to 25 nm, as shown in Fig. 3.

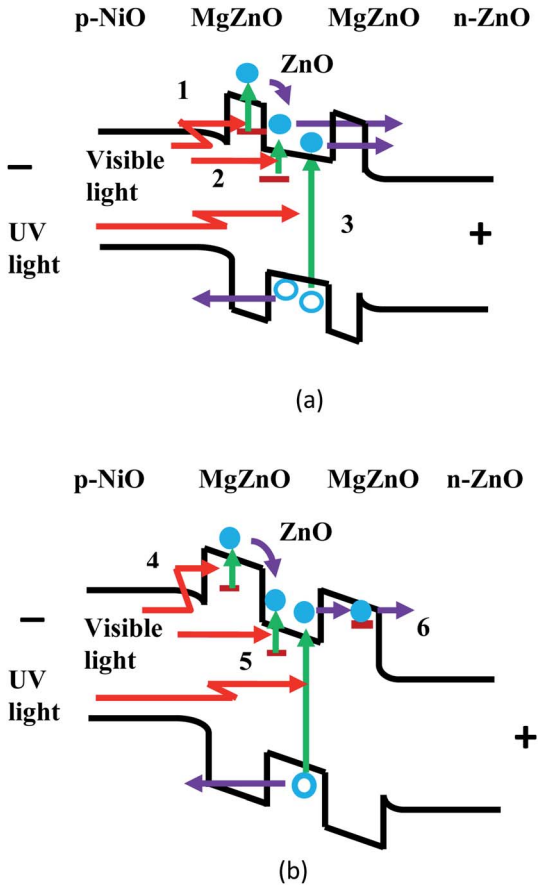


Fig. 7 Band diagrams of QW-PDs with (a) thinner (10 nm) and (b) thicker (≧25 nm) barrier layers, biased at reverse-voltage.

## Conclusions

An $Mg_xZn_{1-x}O$/ZnO QW structure, with various barrier ($Mg_xZn_{1-x}O$ layer) thickness, was inserted into p-NiO/n-ZnO HPDs using a low-cost RF magnetron sputtering system. The effect of the various barrier thickness on the performances of p-NiO/QW/n-ZnO QW-PDs were investigated. The QW-PDs with 10 nm-thick barrier layer presents higher UV and visible responses due to the photo-generated carriers tunnelling through the thin barrier layer. However, in the QW-PDs with thicker (≧25 nm) barrier layer, the carriers generated by visible light are effectively confined within the well layer in the QW structure, causing the visible response to be reduced by more than 3 orders compared to that in the QW-PD with 10 nm barrier layer. By increasing the barrier thickness beyond 25 nm, the visible response will no longer be reduced. In contrast, by decreasing the barrier thickness from 60 to 25 nm, the UV response increases due to the larger overlap of fundamental electron and hole wave function in the quantum well. As a result, the rejection ratio is drastically enhanced from 264 for QW-PDs with 10 nm barrier to 2986 for QW-PDs with 25 nm barrier layer (11.3-fold increase). Based on above investigations, a suitable thickness barrier layer can greatly reduce the visible response and increase the rejection ratio in the p-NiO/QW/n-ZnO HPDs.

## Conflicts of interest

There are no conflicts to declare.

## Acknowledgements

This work was supported by the Ministry of Science and Technology of the Republic of China, Taiwan, under Contract No. MOST 105-2112-M-415-001-MY3.

## References

1 Y. F. Li, B. Yao, R. Deng, B. H. Li, J. Y. Zhang, Y. M. Zhao, D. Y. Jiang, Z. Z. Zhang, C. X. Shan, D. Z. Shen, X. W. Fan and Y. M. Lu, *J. Phys. D: Appl. Phys.*, 2009, **42**, 105102.
2 C. T. Lee, T. S. Lin and C. H. Chen, *J. Electron. Mater.*, 2015, **44**, 4722–4725.
3 J. D. Hwang, D. H. Wu and S. B. Hwang, *IEEE Photonics Technol. Lett.*, 2014, **26**, 1081–1084.
4 L. Su, Y. Zhu, X. Xu, H. Chen, Z. Tang and X. Fang, *J. Mater. Chem. C*, 2018, **6**, 7776–7782.
5 G. Cheng, X. Wu, B. Liu, B. Li, X. Zhang and Z. Du, *Appl. Phys. Lett.*, 2011, **99**, 203105.
6 Y. Z. Li, X. M. Li and X. D. Gao, *J. Alloys Compd.*, 2011, **509**, 7193–7197.
7 H. Zhou, G. Fang, N. Liu and X. Zhao, *Nanoscale Res. Lett.*, 2011, **6**, 147.
8 H. Y. Chen, K. W. Liu, X. Chen, Z. Z. Zhang, M. M. Fan, M. M. Jiang, X. H. Xie, H. F. Zhao and D. Z. Shen, *J. Mater. Chem. C*, 2014, **2**, 9689–9694.
9 S. H. Lee, S. H. Lim and J. S. Yu, *Nanoscale Res. Lett.*, 2016, **11**, 333.
10 R. Liu, D. Jiang, Q. Duan, L. Sun, C. Tian, Q. Liang, S. Gao and J. Qin, *Appl. Phys. Lett.*, 2014, **105**, 043505.
11 J. D. Hwang and G. S. Lin, *Nanotechnology*, 2016, **27**, 375502.
12 Z. G. Ju, C. X. Shan, D. Y. Jiang, J. Y. Zhang, B. Yao, D. X. Zhao, D. Z. Shen and X. W. Fan, *Appl. Phys. Lett.*, 2008, **93**, 173505.
13 H. Zhu, C. X. Shan, L. K. Wang, J. Zheng, J. Y. Zhang, B. Yao and D. Z. Shen, *J. Phys. Chem. C*, 2010, **114**, 7169–7172.
14 W. Yang, S. S. Hullavarad, B. Nagaraj, I. Takeuchi, R. P. Sharma, T. Venkatesan, R. D. Vispute and H. Shen, *Appl. Phys. Lett.*, 2003, **82**, 3424–3426.
15 Y. Zhu, H. Zhou, G. Fang and M. Li, *Semicond. Sci. Technol.*, 2012, **27**, 065003.
16 S. Mridha and D. Basak, *J. Appl. Phys.*, 2007, **101**, 083102.
17 J. M. Nel, F. D. Auret, L. Wu, M. J. Legodi, W. E. Meyer and M. Hayes, *Sens. Actuators, B*, 2004, **100**, 270–276.
18 J. Y. Wang, C. Y. Lee, Y. T. Chen, C. T. Chen, Y. L. Chen, C. F. Lin and Y. F. Chen, *Appl. Phys. Lett.*, 2009, **95**, 131117.
19 Y. Y. Xi, Y. F. Hsu, A. B. Djurišic, A. M. C. Ng, W. K. Chan, H. L. Tam and K. W. Cheah, *Appl. Phys. Lett.*, 2008, **92**, 113505.
20 N. Park, K. Sun, Z. Sun, Y. Jiang and D. Wang, *J. Mater. Chem. C*, 2013, **1**, 7333–7338.
21 A. Echresh, C. O. Chey, M. Z. Shoushtari, V. Khrnovskyy, O. Nur and M. Willander, *J. Alloys Compd.*, 2015, **632**, 165–171.
22 R. Debnath, T. Xie, B. Wen, W. Li, J. Y. Ha, N. F. Sullivan, N. V. Nguyen and A. A. Motayed, *RSC Adv.*, 2015, **5**, 14646–14652.
23 H. Ohta, M. Hirano, K. Nakahara, H. Maruta, T. Tanabe, M. Kamiya, T. Kamiya and H. Hosono, *Appl. Phys. Lett.*, 2003, **83**, 1029–1031.
24 Y. Vygranenko, K. Wang and A. Nathan, *Appl. Phys. Lett.*, 2006, **89**, 172105.
25 J. D. Hwang and W. M. Lin, *IEEE Trans. Nanotechnol.*, 2019, **18**, 126–131.
26 H. Imran, T. M. Abdolkader and N. Z. Butt, *IEEE Trans. Electron Devices*, 2016, **63**, 3584–3590.
27 M. Awais, M. Rahman, J. M. D. MacElroy, N. Coburn, D. Dini, J. G. Vos and D. P. Dowling, *Surf. Coat. Technol.*, 2010, **204**, 2729–2736.
28 A. G. Marrani, V. Novelli, S. Sheehan, D. P. Dowling and D. Dini, *ACS Appl. Mater. Interfaces*, 2014, **6**, 143–152.
29 H. L. Mosbacker, Y. M. Strzhemechny, B. D. White, P. E. Smith, D. C. Look, D. C. Reynolds, C. W. Litton and L. J. Brillson, *Appl. Phys. Lett.*, 2005, **87**, 012102.
30 R. E. Schifano, V. Monakhov, U. Grossner and B. G. Svensson, *Appl. Phys. Lett.*, 2007, **91**, 193507.
31 M. R. Hasan, T. Xie, S. C. Barron, G. Liu, N. V. Nguyen, A. Motayed and M. V. Rao, *APL Mater.*, 2015, **3**, 106101.
32 M. Patel, H. S. Kim and J. Kim, *Adv. Electron. Mater.*, 2015, **1**, 1500232.
33 Y. R. Li, C. Y. Wan, C. T. Chang, W. L. Tsai, Y. C. Huang, K. Y. Wang and P. Y. Yang, *Vacuum*, 2015, **118**, 48–54.
34 C. L. Yu, R. W. Chuang, S. J. Chang, P. C. Chang, K. H. Lee and J. C. Lin, *IEEE Photonics Technol. Lett.*, 2007, **19**, 846–848.
35 S. K. Zhang, W. B. Wang, F. Yun, L. He, H. Morkoç, X. Zhou, M. Tamargo and R. R. Alfano, *Appl. Phys. Lett.*, 2002, **81**, 4628–4630.
36 M. M. Liang, G. E. Weng, J. Y. Zhang, X. M. Cai, X. Q. Lu, L. Y. Ying and B. P. Zhang, *Chin. Phys. B*, 2014, **23**, 054211.
37 S. K. H. Sim, H. C. Liu, A. Shen, M. Gao, K. F. Lee, M. Buchanan, Y. Ohno, H. Ohno and E. H. Li, *Infrared Phys. Technol.*, 2001, **42**, 115–121.
38 J. J. Wierer Jr, D. D. Koleske and S. R. Lee, *Appl. Phys. Lett.*, 2012, **100**, 111119.
39 N. Watanabe, H. Yokoyama, N. Shigekawa, K. I. Sugita and A. Yamamoto, *Jpn. J. Appl. Phys.*, 2012, **51**, 10ND10.
40 L. Redaelli, A. Mukhtarova, A. Ajay, A. Núñez-Cascajero, S. Valdueza-Felip, J. Bieuse, C. Durand, J. Eymery and E. Monroy, *Jpn. J. Appl. Phys.*, 2015, **54**, 072302.
41 G. B. Lin, D. Y. Kim, Q. Shan, J. Cho, E. F. Schubert, H. Shim, C. Sone and J. K. Kim, *IEEE Photonics J.*, 2013, **5**, 1600207.
42 M. Stölzel, J. Kupper, M. Brandt, A. Müller, G. Benndorf, M. Loren and M. Grundmann, *J. Appl. Phys.*, 2012, **111**, 063701.
43 H. R. Chen, C. Y. Tsai, Y. C. Huang, C. C. Kuo, H. C. Hsu and W. F. Hsieh, *J. Phys. D: Appl. Phys.*, 2016, **49**, 095105.

44 T. Makino, C. H. Chia, N. T. Tuan, H. D. Sun, Y. Segawa, M. Kawasaki, A. Ohtomo, K. Tamura and H. Koinuma, *Appl. Phys. Lett.*, 2000, **77**, 975–977.
45 B. Laumer, F. Schuster, T. A. Wassner, M. Stutzmann, M. Rohnke, J. Schörmann and M. Eickhoff, *J. Appl. Phys.*, 2012, **111**, 113504.
46 J. W. Sun, Y. M. Lu, Y. C. Liu, D. Shen, Z. Z. Zhang, B. H. Li, J. Y. Zhang, B. Yao, D. X. Zhao and X. W. Fan, *J. Phys. D: Appl. Phys.*, 2007, **40**, 6541–6544.
47 S. M. Li, B. J. Kwon, H. S. Kwack, L. H. Jin, Y. H. Cho, Y. S. Park, M. S. Han and M. S. Park, *J. Appl. Phys.*, 2010, **107**, 033513.
48 T. Makino, N. T. Tuan, H. D. Sun, C. H. Chia, Y. Segawa, M. Kawasaki, A. Ohtomo, K. Tamura, T. Suemoto, H. Akiyama, M. Baba, S. Saito, T. Tomita and H. Koinuma, *Appl. Phys. Lett.*, 2001, **78**, 1979–1981.
49 M. Brandt, M. Lange, M. Stölzel, A. Müller, G. Benndorf, J. Zippel, J. Lenzner, M. Lorenz and M. Grundmann, *Appl. Phys. Lett.*, 2010, **97**, 052101.
50 J. Zhu, A. Y. Kuznetsov, M. S. Han, Y. S. Park, H. K. Ahn, J. W. Ju and I. H. Lee, *Appl. Phys. Lett.*, 2007, **90**, 211909.
51 S. C. Su, H. Zhu, L. X. Zhang, M. He, L. Z. Zhao, S. F. Yu, J. N. Wang and F. C. C. Ling, *Appl. Phys. Lett.*, 2013, **103**, 131104.
52 J. Zippel, M. Stölzel, A. Müller, G. Benndorf, M. Loren, H. Hochmuth and M. Grundmann, *Phys. Status Solidi B*, 2010, **247**, 398–404.
53 G. Tabares, A. Hierro, M. Lopez-Ponce, E. Muñoz, B. Vinter and J. M. Chauveau, *Appl. Phys. Lett.*, 2015, **106**, 061114.
54 Y. S. Choi, J. W. Kang, B. H. Kim and S. J. Park, *Opt. Express*, 2013, **21**, 31560–31566.
55 X. Mo, G. Fang, H. Long, H. Huang, S. Li, H. Wang and P. Qin, *Semicond. Sci. Technol.*, 2013, **28**, 015016.
56 J. D. Hwang, C. C. Yang and C. M. Chu, *ACS Appl. Mater. Interfaces*, 2017, **9**, 23904–23908.
57 J. D. Hwang and T. H. Ho, *Mater. Sci. Semicond. Process.*, 2017, **71**, 396–400.
58 A. Teke, S. Dogan, F. Yun, M. A. Reshchikov, H. Le, X. Q. Liu, H. Morkoç, S. K. Hang, W. B. Wang and R. R. Alfano, *Solid-State Electron.*, 2003, **47**, 1401–1408.
59 Y. Irokawa, B. Luo, J. Kim, J. R. Larcche, F. Ren, K. H. Baik, S. J. Pearton, C. C. Pan, G. T. Chen, J. I. Chi, S. S. Park and Y. J. Park, *Appl. Phys. Lett.*, 2003, **83**, 2271–2273.
60 J. W. Kang, Y. S. Choi, B. H. Kim, C. G. Kang, B. H. Lee, C. W. Tu and S. J. Park, *Appl. Phys. Lett.*, 2014, **104**, 051120.
61 N. K. Reddy, Q. Ahsanulhaq, J. H. Kim and Y. B. Hahn, *Appl. Phys. Lett.*, 2008, **92**, 043127.
62 R. N. Gayen and S. R. Bjhattacharyya, *J. Phys. D: Appl. Phys.*, 2016, **49**, 115102.
63 R. Ghosh and D. Basak, *Appl. Phys. Lett.*, 2007, **90**, 243106.
64 J. D. Yeh, S. L. Gu, S. M. Zhu, W. Liu, S. M. Liu, R. Zhang, Y. Shi and Y. D. Zheng, *Appl. Phys. Lett.*, 2006, **88**, 182112.
65 R. Mahapatra, A. K. Chakraborty, N. Poolamai, A. Horsfall, S. Chattopadhyay, N. G. Wright, K. S. Coleman, P. G. Coleman and C. P. Burrows, *J. Vac. Sci. Technol., B: Microelectron. Nanometer Struct.–Process., Meas., Phenom.*, 2007, **25**, 217–223.
66 H. Tanaka, S. Fujita and S. Fujita, *Appl. Phys. Lett.*, 2005, **86**, 192911.
67 T. Makino, Y. Segawa, A. Tsukazaki, H. Saito, S. Takeyama, S. Akasaka, K. Nakahara and M. Kawasaki, *Phys. Rev. B: Condens. Matter Mater. Phys.*, 2013, **87**, 085312.
68 J. Aippel, M. Stölel, A. Müller, G. Benndorf, M. Lorenz, H. Hochmuth and M. Grundmann, *Phys. Status Solidi B*, 2010, **247**, 398–404.